

Investigations on the Mechanical, Wear and Corrosion Properties of Cold Metal Transfer Welded and Friction Stir Welded Aluminium Alloy AA2219

M. N. Abijith^a, Adithya Rajeev Nair^a, M. Aadharsh^a, R. Vaira Vignesh^a

R. Padmanaban^{*a}, M. Arivarasu^b

^aDepartment of Mechanical Engineering, Amrita School of Engineering, Coimbatore, Amrita Vishwa Vidyapeetham, India.

^bCenter for Innovative Manufacturing and Research, Vellore Institute of Technology, Vellore, India.

Received 1 August. 2018

Abstract

Aluminium – Copper alloy AA2219 finds application in aerospace and automotive components because of its high strength to weight ratio and corrosion resistance. However, joining of the alloy by conventional welding techniques results in poor property profile. In this study, AA2219 rolled plates of thickness 5.5 mm are joined by cold metal transfer welding process and friction stir welding process. The microstructure, mechanical, corrosion and wear properties of the welded plates are analyzed. The results indicate that cold metal transfer welded specimens have high hardness and tensile strength than the friction stir welded specimens. However, the corrosion resistance and wear resistance of friction stir welded specimens are higher than the base material and cold metal transfer welded specimens.

© 2018 Jordan Journal of Mechanical and Industrial Engineering. All rights reserved

Keywords: Aluminium alloy, Friction stir welding, Cold metal transfer welding, Corrosion, Wear;

Introduction

Aluminium alloys are the preferred materials for light weighting of engineering components. Aluminium – Copper alloy AA2219 is widely used in aerospace and aircraft components because of its good strength to weight ratio and corrosion resistance. The high strength and fracture toughness of AA2219 alloy are attributable to the grain boundary layers [1]. The solidification cracking resistance of AA2219 alloy enabled joining of different components by welding techniques [2, 3]. Though AA2219 alloy has better weldability than other hardenable aluminium alloys, conventional welding results in unfavorable defects such as liquation cracking, porosity, and weldment distortion [4]. For an example, the tensile strength and fatigue strength of conventionally welded AA2219 alloy were much lower than the base material [5-8].

Cold metal transfer welding is one of the emerging areas in welding, which is a modified form of the gas metal arc welding process. During the welding process, at the instance of the electrode wire tip contacting the molten pool, the servomotor reverses the direction of the welding torch and retracts the wire electrode. This enables the fall of a single drop of the molten wire electrode over the joint line. A sound joint is produced by the fusion of wire electrode material and the base material in the weldment.

The advantage of cold metal transfer welding process is its higher electrode melting coefficient than other welding processes [9]. As the current drops to near-zero during the metal transfer, cold metal transfer welding has less spattering effect compared to other short-circuit welding techniques [10]. Hence, the wire feed rate affects the phase duration and short-circuit duration. An increase in the short-circuit duration increases the grain size of the post-welded material [11] and slow welding speeds lead to the formation of heat-affected zone, which increases the vulnerability to liquation cracking [12].

In this study, the AA2219 alloy plates were cold metal transfer welded by varying the process parameters (welding current and welding speed). Defect-free joint with high depth of penetration was chosen as the criteria for optimizing the cold metal transfer welding process parameters. To assess the performance of the cold metal transfer welded AA2219 alloy plates, AA2219 alloy plates were joined by the friction stir welding process. The friction stir welding process is one of the preferred industrial techniques for welding AA2219 alloy. In this process, a rotating non-consumable tool is plunged into the workpiece and traversed along the welding line. The action of load and traverse of the rotating tool in the workpiece generates frictional heat, which plasticizes the material enabling a joint in the solid state [13, 14]. Friction stir welding process parameters significantly influence the evolution of microstructure and henceforth the properties

of the weldments [15]. The incorporation of right welding parameters avoids melting of aluminium alloys, reduce the formation of intermetallic compounds and help to achieve desirable properties [16]. Friction stir welded aluminium alloys have negligible issues such as cracking and porosity when compared to other arc welding techniques [17-19]. The microstructural constituents in cold metal transfer welded and friction stir welded specimens were characterized using microstructural analysis and X-ray diffraction analysis. The microhardness, tensile strength, and impact strength of the welded plates were evaluated. The fractograph of the tensile and impact test specimens were obtained using field emission – scanning electron microscope to deduce the fracture mechanism. The surface morphology of the specimens post corrosion and wear test was observed using field emission - scanning electron microscope to understand the corrosion mechanism and wear mechanism. This article presents a comparative study on the performance of the AA2219 alloy plates joined by cold metal transfer welding and friction stir welding process.

Materials and Methods

Material

Aluminium alloy AA2219 forged plate of thickness 5.5 mm was used in this study. The alloy was received in the annealed condition and its chemical composition is given in Table 1.

Table 1. Composition of AA2219

Element	Mn	Mg	Fe	Si	Cr	Zn	Ti	Cu	Al
Composition (Weight %)	0.229	0.007	0.108	0.079	0.130	0.046	0.040	5.959	Balance

Cold metal transfer welding

The AA2219 alloy plate was cut into workpieces of dimension 150 mm × 50 mm × 5.5 mm and degreased using acetone. The bead on trials and experimental welding trials were carried out using Fronius cold metal transfer welding machine. Aluminium alloy AA4024 wire of diameter 1.2 mm was used as filler material for the cold metal transfer welding process. Argon gas at a flow rate of 15 liters.min⁻¹ shielded the weld pool from the atmosphere. The filler wire was fed at a rate of 7.6 m.min⁻¹ and the stick out distance was 10 mm. The cold metal transfer welding trials were performed by varying the current and welding speed as per the experimental layout in Table 2. The penetration depth of the weldments is measured at each parametric combinations of current and welding speed.

Table 2. Process parameters for bead-on trials of AA2219 (Cold metal transfer welding)

Sl.	Current (A)	Speed mm.min ⁻¹	Depth of Penetration (mm)	Sl.	Current (A)	Speed mm.min ⁻¹	Depth of Penetration (mm)
1	70	800	0.550	11	132	1000	0.930
2	70	900	0.640	12	148	800	1.370
3	70	1000	0.900	13	148	1000	1.220
4	80	800	0.450	14	162	800	1.680
5	80	900	0.680	15	170	700	3.660
6	80	100	1.000	16	170	800	2.780
7	90	800	0.450	17	170	900	2.440
8	90	900	0.590	18	170	1000	1.830
9	90	1000	0.790	19	180	700	3.240
10	132	800	1.180				

Friction stir welding

The friction stir welding trials were performed by varying the welding speed as per the experimental layout in Table 3. The workpieces were cleaned and degreased with acetone. Friction stir welding trials were carried out in friction stir welding competent computer numerical control milling machine. The experimental procedures to perform friction stir welding trials were discussed elsewhere [20, 21].

Table 3. Experimental layout of Friction Stir Welding trials

Sl.	Tool rotation speed (rpm)	Welding Speed (mm.min ⁻¹)	Plunge depth (mm)
1	1600	45	5.3
2	1600	60	5.3
3	1600	75	5.3

Microstructural analysis

The specimens for microstructural analysis were cut from the base material, cold metal transfer welded workpiece and friction stir welded workpiece. The cut specimens were prepared and polished as per the ASTM E3-11 standard. The etchant was prepared, and the specimens were etched as per the guidelines of the ASTM E407-07 standard. The microstructure of the specimens was observed using an optical microscope (Carl Zeiss).

Mechanical tests

The specimen for microhardness test was prepared from the base material, cold metal transfer welded workpiece and friction stir welded specimens according to the IS 1501:2002 standard. Vicker's microhardness was measured using a microhardness tester (Mitutoyo) with a test load of 50 N for a time period of 10s. Three tensile test specimens were fabricated from each of the base material, cold metal transfer welded workpiece and friction stir welded workpiece as per the ASTM E8/8M-15a standard. The tensile strength was calculated from the stress-strain graph, which was obtained from the computerized tensile testing machine (Tinius Olsen). For measuring the maximum impact load, three specimens each from the base material, cold metal transfer welded workpiece and friction stir welded workpiece were prepared and subjected to Charpy impact test as outlined by the ASTM E23-12c standard.

Wear test

The specimens were cut from the base material, cold metal transfer welded workpiece and friction stir welded workpiece and were mounted in a hollow steel tube using a cold setting compound. The wear test was conducted as per the ASTM G99-95a standard, in a pin on disc tribometer (Duom) with the specimen as pin and counter disc made of EN316 steel. The wear test parameters were chosen as follows: track diameter of 60 mm, sliding velocity of 1.5 m.s⁻¹ and sliding distance of 900 m. An uninterrupted contact was established between the specimen and the counter disc by applying a load of 9.80 N through a lever system. The mass of the specimens before and after the wear test was measured using a precision balance of readability 0.0001 g.

Corrosion tests

Immersion corrosion test

The specimens were prepared from the base material, cold metal transfer welded workpiece and friction stir welded workpieces as per the directions outlined in the Microstructure section. The specimens were cleaned and subjected to immersion test as per the ASTM G31-72 standard. The immersion tests were performed in artificial seawater solution (3.5 weight % sodium chloride solution) at room temperature T1 = 27°C and at an elevated temperature T2 = 45°C. The temperature of the solution was maintained using a water bath, which was fitted with a digital temperature controller with a sensitivity of 0.1°C. After the immersion period, the corrosion products were cleaned using the cleaning solution as per the ASTM G1-03 standard. The cleaning solution was prepared by mixing 25 ml of phosphoric acid and 10 g of chromium trioxide in 500 ml of water. The specimens were immersed in the cleaning solution (heated and maintained at 80°C) for 300 s, to remove all the corrosion products. Then the specimens were rinsed in nitric acid for 60 s. The specimens were dried in a blast of hot air and then weighed in the precision balance of readability 0.0001 g to calculate the mass loss of the specimens.

Electrochemical corrosion test

Electrochemical corrosion tests were performed for the base material and the workpieces welded by both cold metal transfer welding and friction stir welding techniques to calculate their corrosion potential and corrosion current in artificial seawater solution. The specimens were prepared as per the ASTM G102 standard. The surface of the specimens was prepared as described in the *Microstructure section*. The specimens were masked using an insulation tape, such that an area of 1 mm² was exposed to the electrolyte (artificial seawater solution). Electrochemical cell setup was built using calomel electrode as the reference electrode, a platinum wire as the counter electrode and the specimen as the working electrode. The electrodes were connected to the electrochemical workstation (CH Instruments). An open circuit potential was established for each specimen and the

specimens were potentiodynamically polarized with reference to open circuit potential at a scan rate of 5 mV.s⁻¹.

Surface morphology, Elemental composition, Phase analysis

The specimens subjected to wear and corrosion test were preserved in a desiccator. The surface morphology of the specimens was observed using field emission scanning electron spectroscopy (Zeiss Sigma). The images were obtained at an electron acceleration potential of 10kV and a wide range of magnifications. The elemental composition of the worn out and corroded specimens were analyzed using energy-dispersive X-ray spectroscopy (Bruker). The spectra were obtained at an electric acceleration potential of 20kV over a small region of the corroded specimen. The X-ray diffractometer (Rigaku) was used to analyze the constitutional phases present in the cold metal transfer welded workpiece and friction stir welded workpiece using Copper-K α radiation in continuous scanning mode at a scan rate of 2° min⁻¹.

Results and Discussions

Macrostructure

Cold Metal Transfer Welding

Cold metal transfer welding trials were conducted by varying the cold metal transfer welding process parameters (welding current and welding speed). The corresponding penetration depth of the weldments was measured and given in Table 2. The mathematical relationship between the process variables and response variables could be devised using a standard statistical regression equation [22]. However, the penetration depth exhibited complex non-linear characteristics with cold metal transfer welding the process parameters. Hence, a hybrid model integrating the polynomial function and radial basis function was developed to relate the cold metal transfer welding process parameters (welding current and welding speed) with the response variable (depth of penetration) using Matlab ® technical computing environment. The details regarding the development of model are discussed elsewhere [23]. Since the input variables are discrete, a multiquadratic variant of radial basis function model was used. The radial basis function had two centers, a global width of 0.029147 and the regularization parameter was 0.0001. The developed polynomial – radial basis function model using coded levels of welding current (I) and welding speed (S) is given in equation (1).

$$\begin{aligned} \text{Depth of penetraion} &= 0.13896 + 1.5654 \times I \\ &- 0.51265 \times S + 0.27861 \\ &\times I^2 - 0.7344 \times I \times S \\ &- 0.34034 \times S^2 + RBF \end{aligned} \quad (1)$$

Where RBF is radial basis function.

The coefficient of determination (R²) and root mean squared error (RMSE) values of the developed model were 0.98 and 0.064 respectively. The closeness of coefficient of determination to 1 and root mean squared error value to

0, indicates that the developed model is efficient in prediction [23]. Figure 1 shows the contour plot depicting the influence of welding current and welding speed on the penetration depth of the welds. The heat input to the material is proportional to the magnitude of current. Therefore, the high magnitude of welding current melted the material along its depth to a greater extent than the low magnitude of welding current. It is observed that penetration depth increased with increase in welding current from 70 A to 170 A. However, a welding current greater than 170 A resulted in visible weld defects. Hence the experimental trials were limited to welding current of 170 A. Heat input has an inverse relationship with the welding speed. At higher welding speed of 800 mm·min⁻¹, 900 mm·min⁻¹, and 1000 mm·min⁻¹, the amount of heat generated was insufficient to melt the material. So, the specimens processed at high welding speed had low penetration depth, at any level of current. A maximum penetration of 3.66 mm was obtained for 170A welding current and welding speed 700 mm·min⁻¹. Hence, they were chosen as optimum process parameter for cold metal transfer welding of AA2219. At this optimum parametric condition, the specimens were joined by cold metal transfer welding (push method and drag method). For the same penetration depth, the specimen welded by drag method had lesser porosity compared with the specimen welded by push method. Hence, it is established that the drag method is the best choice for cold metal transfer welding of AA2219 alloy (square butt configuration). Repeating the drag method cold metal transfer welding process on the other side of the plate resulted in a complete penetration of 5.5 mm. No visible defects were observed in the macro-structure of the cold metal transfer welded specimen as shown in Figure 2 (a).

Friction Stir Welding

Friction stir welding of the AA2219 alloy at a low

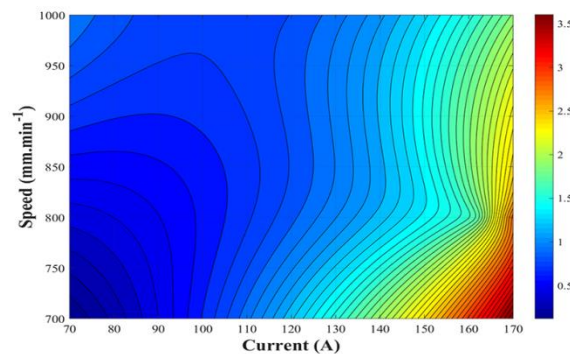


Figure 1. Effect of current and welding speed on the depth of penetration in cold metal transfer welding process

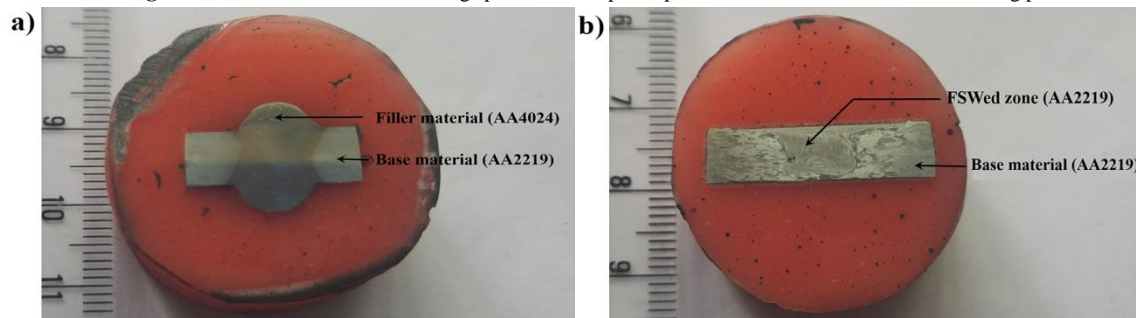


Figure 2. Macrostructure of (a) Cold metal transfer welded specimen (b) Friction stir welded specimen

welding speed of 45 mm·min⁻¹ resulted in visible surface defects and a high welding speed of 75 mm·min⁻¹ resulted in incomplete penetration. A complete penetration and defectless weld were obtained in a single automated pass with at tool rotation speed of 1600 rpm and a welding speed of 60 mm·min⁻¹, as shown in Figure 2 (b). Hence, the optimum friction stir welding process parameters for joining AA2219 alloy is established as follows: tool rotation speed of 1600 rpm and a welding speed of 60 mm·min⁻¹.

Microstructure

Figure 3 (a) shows the dispersed Al₂Cu particles (dark region) in irregular shapes and sizes in the microstructure of the base material. The needle-like continuous structures in the microstructure of AA4024 alloy corresponds to secondary β-(Al, Fe, Si) precipitates (dark region), as shown in Figure 3 (b). Figure 3 (c) shows a clear distinguished weld interface between the matrix of filler material and base material. The microstructural image shows Al₂Cu of the base material, weld interface and β-(Al, Fe, Si) precipitates of the filler material in the cold metal transfer weld specimen. In friction stir welded specimen, the Al₂Cu particles are dispersed on the surface of the and no significant change was observed in the dispersion of Al₂Cu particles, as observed in Figure 3 (d). In X-ray diffraction, the cold metal transfer welded specimen produced significant peaks corresponding to distinct phases α-Al, Al₂Cu, and β-(Al, Fe, Si), as shown in Figure 4 (a). It corresponds to the phases present in the base material (AA2219) and filler material (AA4024). The X-ray diffraction analysis of the friction stir welded specimen revealed the presence of two distinct phases in the matrix α-Al and Al₂Cu, as shown in Figure 4 (b). The X-ray diffraction results are consistent with the aforesaid microstructural analysis.

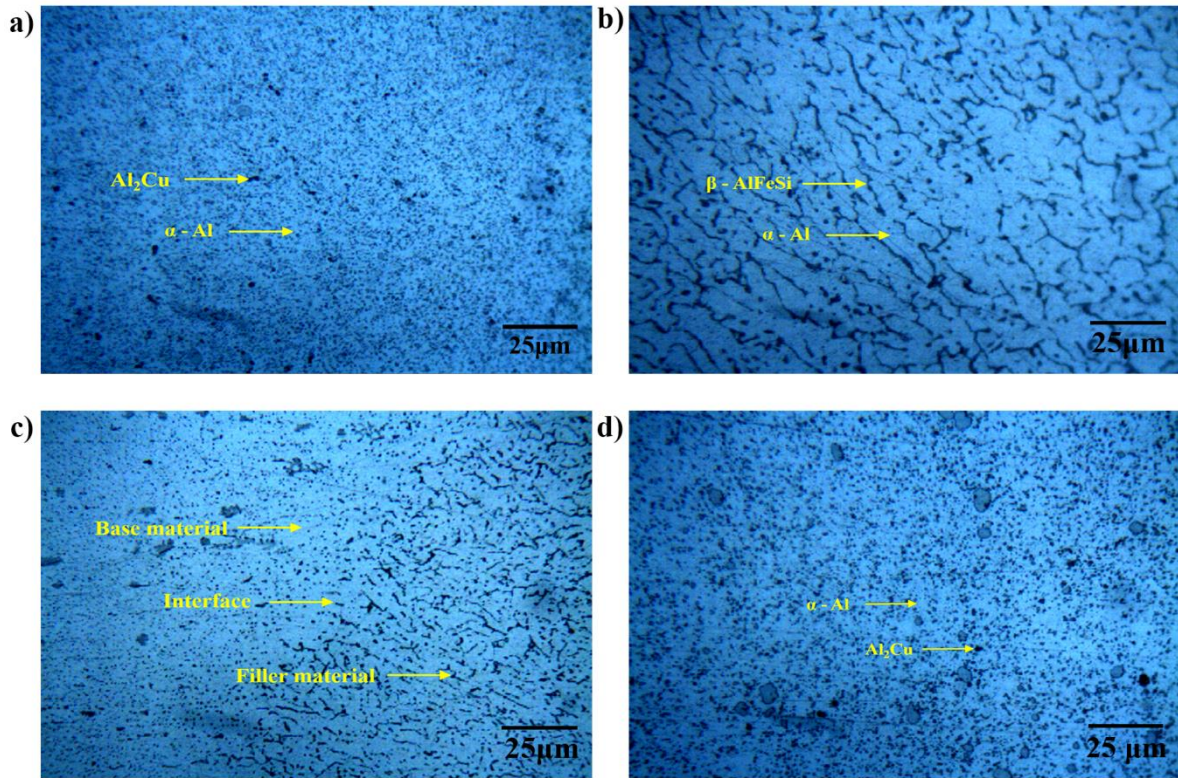


Figure 3. Microstructure of (a) Base material AA2219 (b) Filler material AA4024 (c) Cold metal transfer welded specimen (d) Friction stir welded specimen

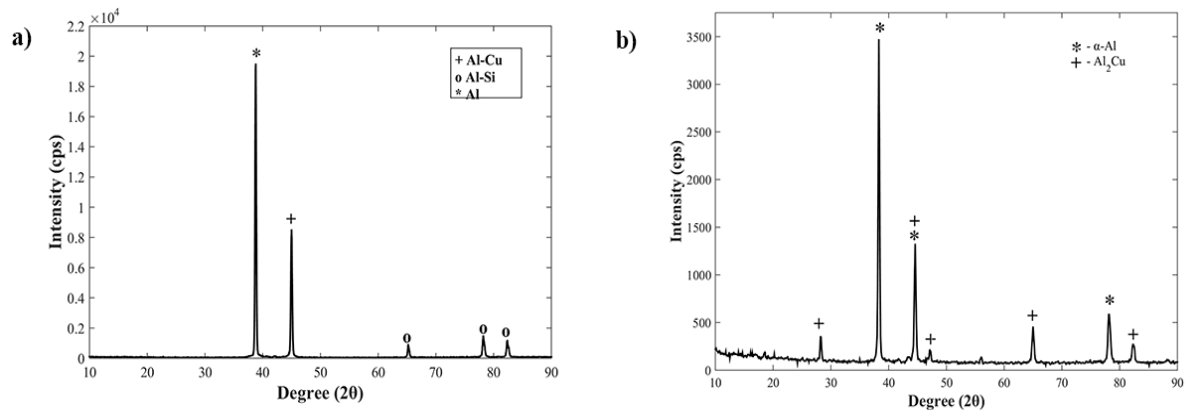


Figure 4. X-ray diffraction analysis of (a) Cold metal transfer welded specimen (b) Friction stir welded specimen

Microhardness

The microhardness of the base material was measured to be 82 Hv. The high microhardness is attributed to Al_2Cu particles in the matrix, which were obstacles for dislocation motion. As observed in the microstructure of cold metal transfer welded specimen, the volume fraction of intermetallic is comparatively higher in the weld zone and weld interface than the base material and filler material. These intermetallic phases acted as barriers to dislocation movement, which increased the microhardness of the material. Hence, the weld zone and weld interface had a higher average microhardness of 110 Hv and 140 Hv respectively. The variation in microhardness of the cold metal transfer welded specimen at the cap-section, mid-section, and root-section of the weldment is shown in Figure 5(a). In the case of the friction stir welded specimens, the microhardness was ~20% lesser than the

microhardness of base material. The partial dissolution of Al_2Cu phase attributes to the low microhardness of the friction stir welded region than the base material. The microhardness plot of the friction stir welded specimen is shown in Figure 5 (b). The microhardness test indicates that the microhardness of cold metal transfer welded specimen is ~41% higher than the microhardness of the friction stir welded specimen.

Tensile Strength

The tensile strength of the specimens was determined using the tensile testing machine and the results are presented in Table 4. The load was applied axially to the tensile test specimens until there was a visible rupture. The average tensile strength and rupture load of the base material specimen were found to be 158.20 MPa and 5.525 kN respectively. The tensile fractograph of the base

material is shown in Figure 6 (a), which revealed a few secondary cracks and dimple features. However, a quite large deformation zone was observed indicating a high tensile strength. The average tensile strength of the friction stir welded specimen was found to be 86.975 MPa and the average load at rupture was found to be 3.0375kN. The tensile fractograph of the friction stir welded specimen indicates the presence of cracks and quasi-cleavage dimples, as shown in Figure 6 (b). The small deformation zone and wide cracks indicated the least tensile strength of the friction stir welded specimen. The average tensile strength and the average load at rupture of the cold metal transfer welded specimen were found to be 159.02 MPa and 5.553 kN respectively. It is observed that the tensile strength of cold metal transfer welded specimen was ~83% higher than the tensile strength of friction stir welded specimens. A large deformation zone with quasi-cleavage dimples was observed in the tensile fractograph of the cold metal transfer welded specimen, as shown in Figure 6 (c). This demonstrated the highest tensile strength of the cold metal transfer welded specimen. Aforesaid microstructural analysis revealed the presence of huge volume fraction of secondary phases in the cold metal transfer welded specimen, which accounted for its high tensile strength. The tensile test results indicate that the cold metal transfer weldments had the higher ultimate tensile strength and rupture load.

Impact strength

The average impact strength of the base material was calculated to be 0.3123 J.mm². As observed Figure 7 (a), the impact fractograph of the base material displayed a comparatively smaller deformation zone, more cleavage steps and tearing ridges than the fractograph of friction stir welded specimens and cold metal transfer welded specimens. It is observed that average impact strength of friction stir welded specimen was 0.3209 J.mm². As shown in Figure 7 (b), more tearing ridges were observed in the impact fractograph of the friction stir welded specimen than the tensile fractograph of the friction stir welded specimen. Many cleavage steps and small deformation zone indicated the lowest impact strength of the friction stir welded specimen. In line with the observations of tensile strength, the impact strength of cold metal transfer welded specimens was higher than the impact strength of the base material and friction stir welded specimens. The average impact strength of cold metal transfer welded specimen was observed to be 0.4242 J.mm². It is attributed to the strong bonding of the filler material with the base material. Figure 7 (c) shows the impact fractograph of the cold metal transfer welded specimen. Quasi-cleavage dimples and large deformation zone indicated quasi-cleavage fracture feature in the cold metal transfer welded specimen, which demonstrated the highest impact strength of the cold metal transfer welded specimens.

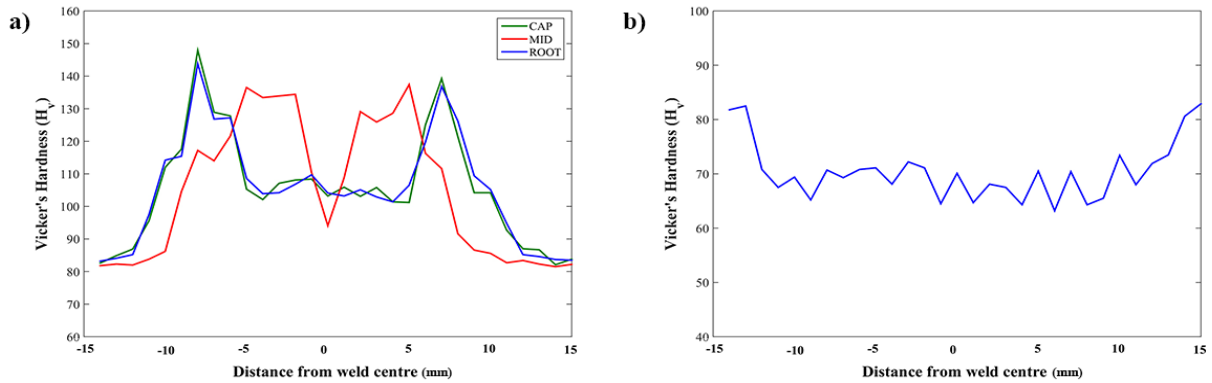


Figure 5. Microhardness plot of (a) Cold metal transfer welded specimen (b) Friction stir welded specimen

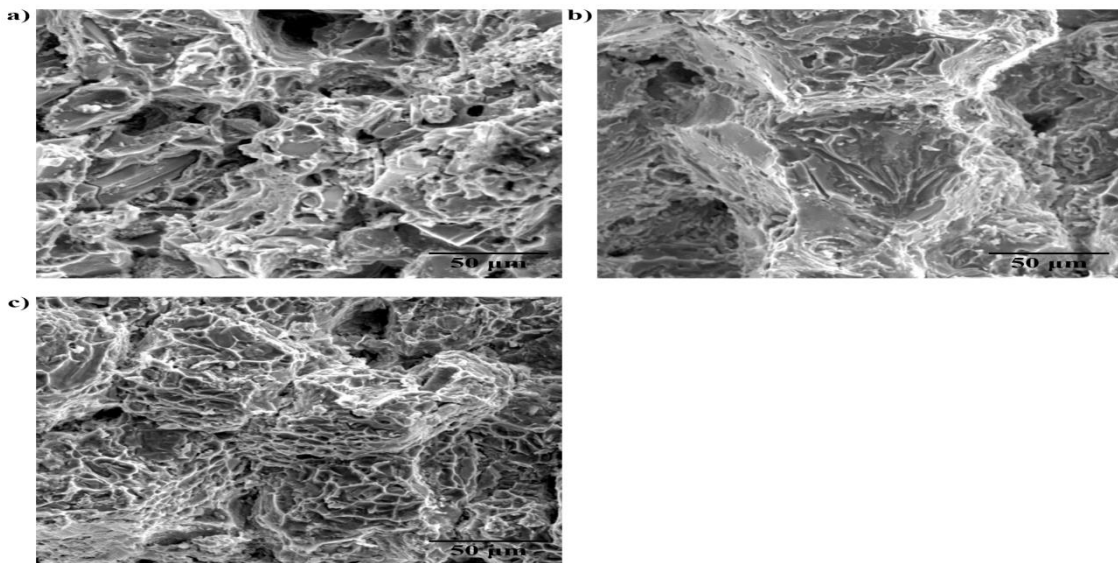


Figure 6. Tensile Fractograph of (a) Base material (b) Friction stir welded specimen (c) Cold metal transfer welded specimen

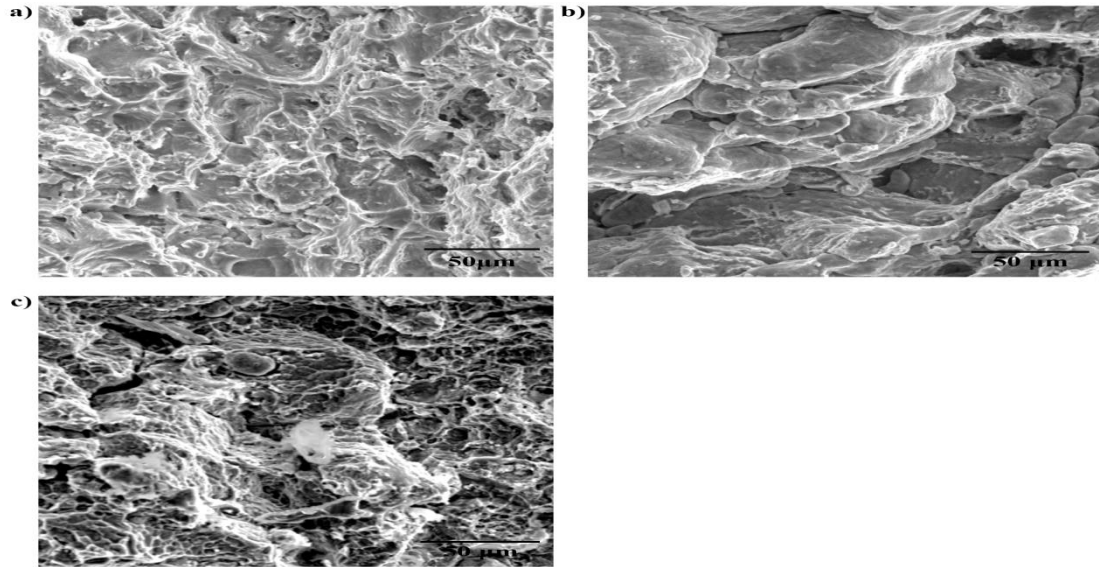


Figure 7. Impact Fractograph of (a) Base material (b) Friction stir welded specimen (c) Cold metal transfer welded specimen

Table 4. Summary of the mechanical, tribological and corrosion tests performed on the base material, cold metal transfer welded and friction stir welded specimen

Sl.	Specimen	Ultimate Tensile Strength (MPa)	Impact Strength (J.mm ⁻²)	Wear rate (×10 ⁻⁷ kg.N ⁻¹ .m ⁻¹)	Corrosion test			
					Immersion test		Potentiodynamic polarization	
					Corrosion rate (10 ⁻⁵ mm/year)		Corrosion potential (V)	Corrosion current (×10 ⁻³ A)
					27°C	45°C		
1	Base material	158.483± 1.431	0.312± 0.019	2.906± 0.628	2.856± 0.040	5.711± 0.090	-(0.559± 0.004)	5± 0.224
2	Cold metal transfer welded specimen	159.020± 1.145	0.425± 0.022	2.802± 0.328	2.128± 0.034	8.820± 0.136	-(0.621± 0.004)	14.643± 1.905
3	Friction stir welded specimen	86.975± 0.495	0.321± 0.015	4.213± 0.296	2.094± 0.027	3.822± 0.066	-(0.601± 0.012)	6.003± 0.127

Wear rate

The wear test was conducted for the base material, cold metal transfer welded and friction stir welded specimens and the wear rate of the specimens was calculated using equation (2) [21]. The wear rate of the specimens is summarized in Table 4.

$$Wear\ rate = \frac{\Delta m}{F \times L} \left(\frac{g}{Nm} \right) \tag{2}$$

Where Δm is mass loss in g, F is load in N and L is sliding distance in m.

A minimum wear rate of 2.905×10^{-7} g/(Nm) was observed for the base material, closely followed by the cold metal transfer welded specimen. The surface morphology of the worn cold metal transfer welded specimen is shown in Figure 8 (a). Loose wear debris and feeble wear tracks were observed on the worn out region, as the result of delamination of the surface oxide layer and

subsurface material layer (adhesive wear). The friction stir welded specimens exhibited the highest wear rate and lowest wear coefficient. The wear track was prominent and the surface had deep continuous grooves on the surface as observed in Figure 8 (b). The worn surface had massive deformation and a large amount of wear debris, which indicated the domination of severe wear regime (abrasive wear). The softness of the matrix, as evident from the hardness test results, resulted in high wear rate of the specimens [24]. It is observed that wear coefficient of the base material and the cold metal transfer welded specimen was more fluctuating in comparison to the friction stir welded specimen. The fluctuation in the cold metal transfer welding specimen was attributed to the more fraction of hard intermetallics in the matrix. In the base material, the frequency of fluctuation was low in the initial phases and increased towards the end. The results indicate that cold metal transfer welded specimens had high wear resistance.

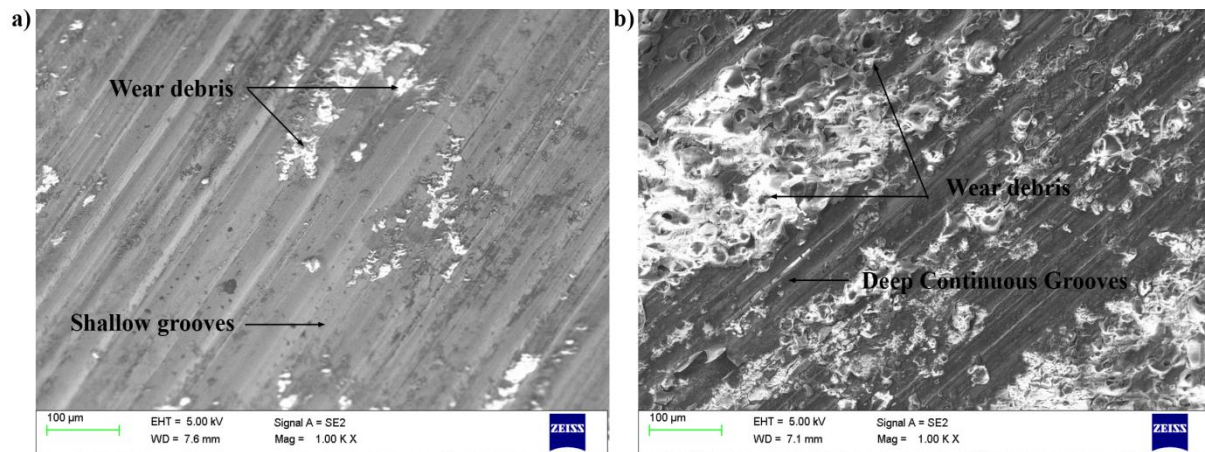


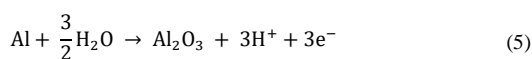
Figure 8. Worn out surface of (a) Cold metal transfer welded specimen (b) Friction stir welded specimen

Corrosion

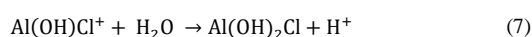
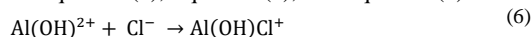
Immersion corrosion

The immersion corrosion test was performed at room temperature and at an elevated temperature of 45°C. The corrosion rate of the specimens (base material, friction stir welded specimen and cold metal transfer welded specimen) was calculated from the mass loss of the specimens and displayed in Table 4. The corrosion rate of the base material at room temperature was 2.8549×10^{-5} mm/year. The corrosion rate decreased by ~25% in both friction stir welded specimen and the cold metal transfer welded specimen at room temperature. It is observed that increase in temperature increased the corrosion rate of the specimens. At the elevated temperature, cold metal transfer welded specimens exhibited the highest corrosion rate of 8.8350×10^{-5} mm/year. The corrosion rate of the cold metal transfer welded specimen was ~54% higher than the base material at elevated temperature. The friction stir welded specimen exhibited the least corrosion rate of 3.8142×10^{-5} mm/year at elevated temperature, which is ~32% lesser than the corrosion rate of the base material at elevated temperature.

The corrosion mechanism of the specimens is described as follows. Aluminium reacts with water as described by the Equation (3), Equation (4) and Equation (5) [23].



But the aggressive chloride ions in the electrolyte transforms aluminium hydroxide to aluminium chloride as per the Equation (6), Equation (7), and Equation (8).



Aluminium hydroxide is transformed into $\text{Al}(\text{OH})_2\text{Cl}$ in the presence of chloride ion, as given by Equation (7). Hydrolysis of $\text{Al}(\text{OH})\text{Cl}^+$ yields an unstable compound, which on further reaction with chloride ion forms aluminium chloride, as per the Equation (8). Aluminium chloride dissolves into solution and exposes a fresh area of

the metal surface to the electrolyte. This process of salt formation, its dissolution, and exposure to fresh surface increase the corrosion rate of the specimen. Figure 9 (a) shows the corroded surface of the base material, which showed the striations on the surface. In agreement with the highest corrosion rate, the cold metal transfer welded specimen had many cracked layers on the surface, as shown in Figure 9 (b). The friction stir welded specimen had the least corrosion rate among the tested specimens. Hence, meager corrosion products were observed on the surface as shown in Figure 9 (c). The results indicate that the corrosion resistance of friction stir welded specimen is higher than the corrosion resistance of cold metal transfer welded specimen.

Electrochemical corrosion

The corrosion characteristics of the base material, cold metal transfer welded and friction stir welded plates were studied using potentiodynamic polarization technique. The Tafel plots for the specimens are shown in Figure 10, which sufficiently prove that pitting occurs only at very high positive potentials. The corrosion current and corrosion potential were extrapolated from the Tafel region and presented in Table 4. The formation of aluminium oxide layer limits the flow of current, decreasing the corrosion rate. The corrosion potential of the base material is nobler (more positive) than the cold metal transfer welded and friction stir welded specimens. Comparing the welding techniques, friction stir welded specimen exhibited a noble corrosion potential of -0.585 V. The cold metal transfer welded specimen exhibited the highest corrosion potential of -0.615 V. The anodic reaction on the surface of the specimen is the formation of aluminium ion, as per the Equation (9).



The principal cathodic reaction in pitting corrosion of aluminium-magnesium alloys, in the marine environment, is the formation OH^- ions [25]. The cathodic reaction is the reduction of atmospheric oxygen in the electrolyte, as per the Equation (10).



The existence of a potential difference between the intermetallics and the matrix created local galvanic sites, which decreased the corrosion potential of cold metal

transfer welded specimens. This is attributed to the high-volume fraction of intermetallic present in the cold metal transfer welded specimen than the base materials and friction stir welded specimen. The cold metal transfer welded specimen had more corrosion products than the base material and friction stir welded specimens, as observed in Figure 11. Pitting corrosion is the dominant mechanism in the corrosion of cold metal transfer welded specimen. The energy dispersive X-ray spectroscopy analysis justified that the corrosion products consisted of aluminium, copper, silicon, sodium, oxygen, and chlorine atoms. The EDS spectra are shown in Figure 12 and Table

5 shows the elemental composition of the corrosion products. The probable corrosion products are chlorides of aluminium, copper, and oxides of aluminium, copper, silicon. Sodium came from the electrolyte, which was made by dissolving the sodium chloride in distilled water. The predominant corrosion product in base material and friction stir welded specimen is aluminium chloride as evidenced by a higher concentration of aluminium and chlorine. The electrochemical corrosion test also reveals that the corrosion resistance of friction stir welded specimen is higher than the corrosion resistance of the cold metal transfer welded specimen.

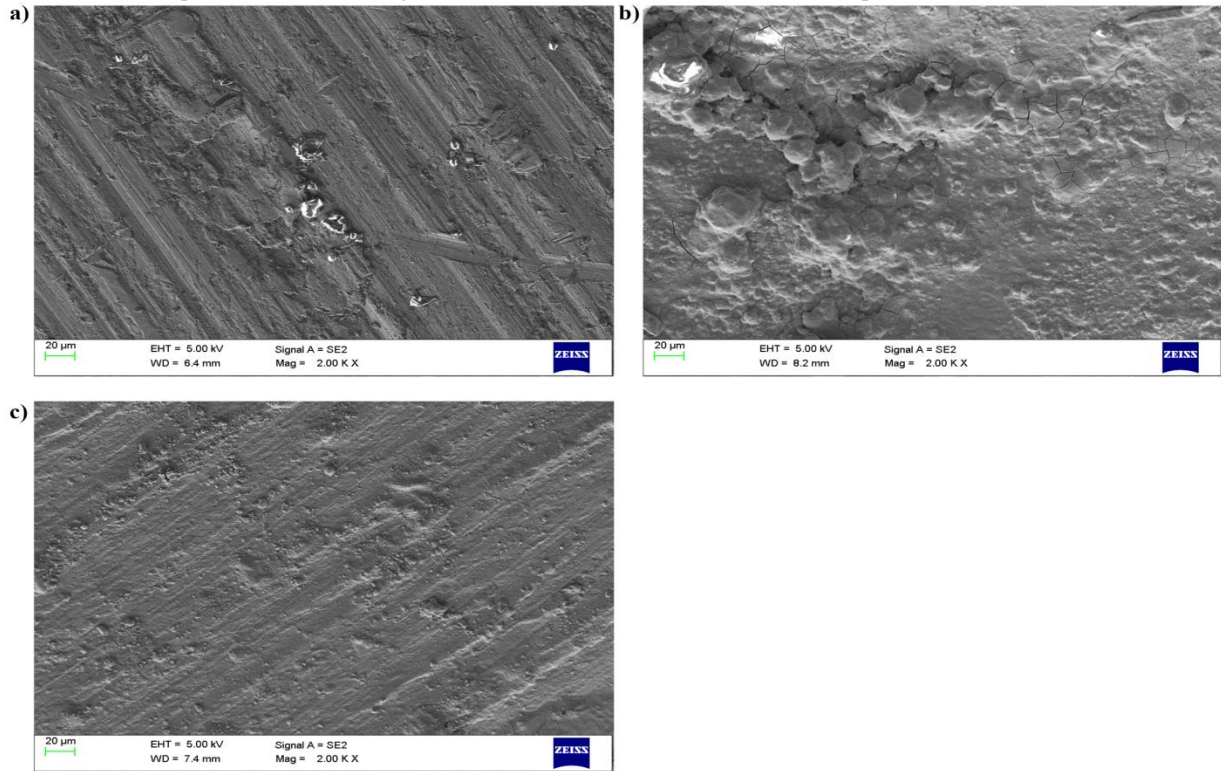


Figure 9. Surface morphology of the corroded (a) Base material (b) Cold metal transfer welded specimen (c) Friction stir welded specimen

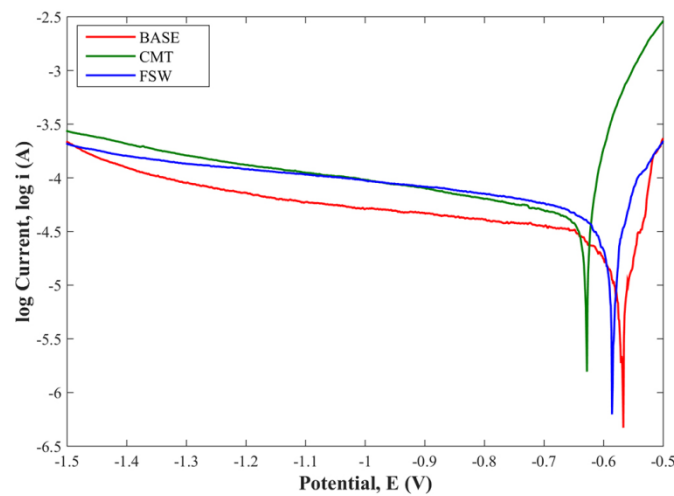


Figure 10. Tafel plot of the base material, Cold metal transfer welded and Friction stir welded specimens

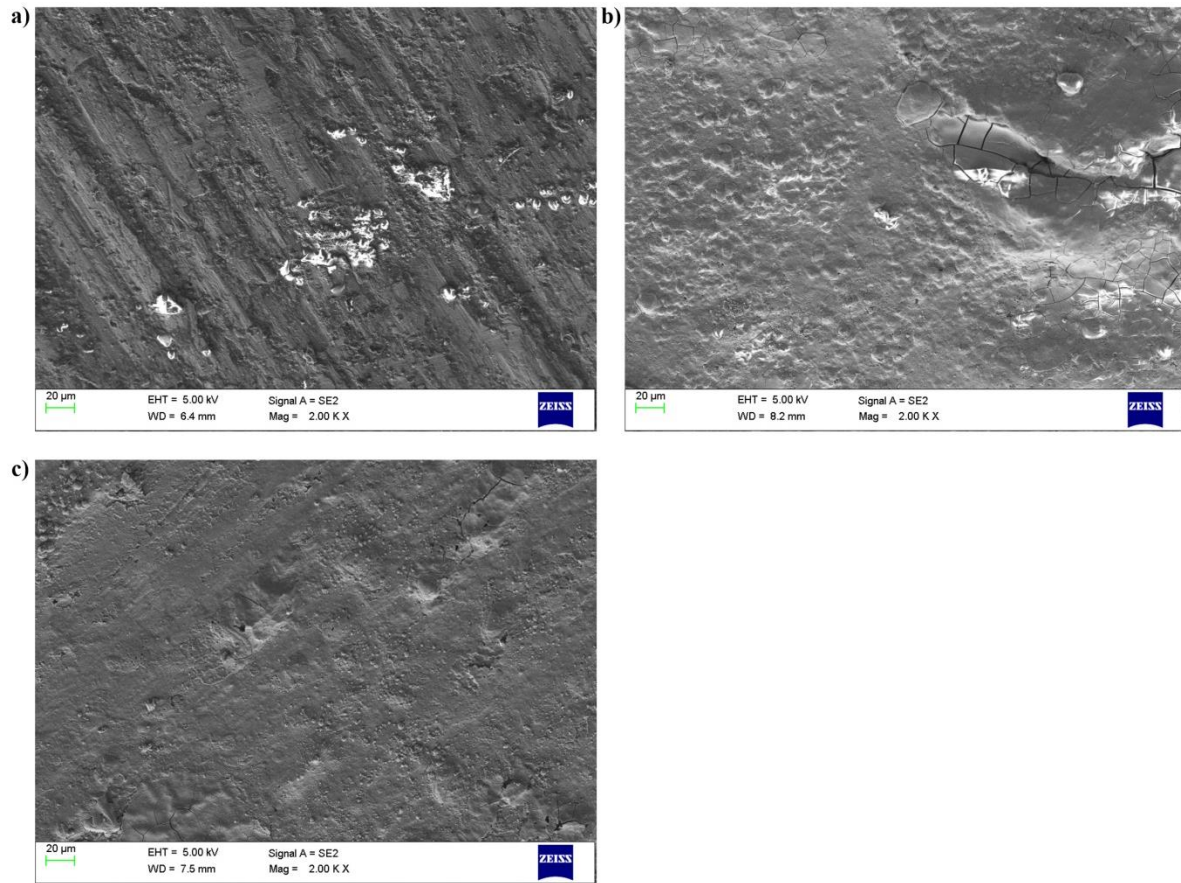


Figure 11. Surface morphology of the corroded (a) Base material (b) Cold metal transfer welded specimen (c) Friction stir welded specimen

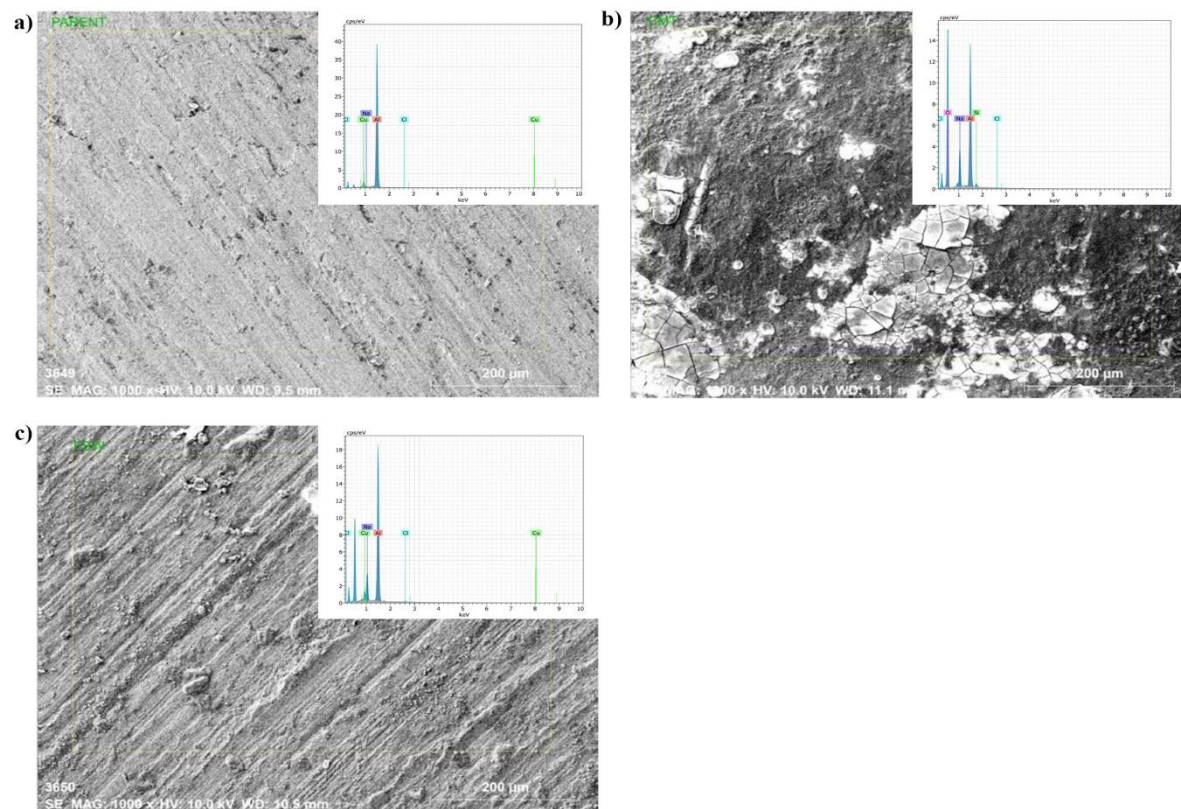


Figure 12. Energy dispersive X-ray spectroscopy analysis of the corroded specimens (a) Base material (b) Cold metal transfer welded specimen (c) Friction stir welded specimen

Table 5. Energy dispersive X-ray analysis of the corroded specimens

Sl.	Element	Normalized concentration			Atomic concentration			Error (3 σ)		
		Wt. %			Wt. %			Wt. %		
		Base	CMTW	FSW	Base	CMTW	FSW	Base	CMTW	FSW
1	Aluminium	92.49	36.79	77.47	96.40	26.83	80.01	10.97	3.83	5.67
2	Copper	7.07	-	9.05	3.13	-	3.97	2.81	-	2.22
3	Sodium	0.29	9.59	12.72	0.35	8.21	15.42	0.14	1.38	1.30
4	Chlorine	0.16	0.19	0.76	0.13	0.11	0.60	0.11	0.11	0.15
5	Silicon	-	1.63	-	-	1.14	-	-	0.26	-
6	Oxygen	-	51.80	-	-	63.71	-	-	13.56	-
Total		100	100	100	100	100	100	100	-	-

CMTW – Cold Metal Transfer Welding; FSW – Friction Stir Welding

Conclusion

Aluminium alloy 2219 plates were welded by cold metal transfer welding and friction stir welding process. The weldments were characterized for microstructure, microhardness, tensile strength, rupture load, impact strength, wear rate, and corrosion rate. The results demonstrated the following.

- The optimum parameters for complete penetration in cold metal transfer welding process were current of 170 A and welding speed of 700 mm.min⁻¹. The optimum parameters for complete penetration in friction stir welding process were tool rotation speed of 1600 rpm and a welding speed of 60 mm.min⁻¹. The results demonstrated the following.
- The microstructure of the base material AA2219 had Al₂Cu particles, cold metal transfer welded specimens had Al₂Cu and β -(Al, Fe, Si) particles. The friction stir welded specimens had Al₂Cu particles.
- The microhardness of the cold metal transfer welded specimens were found to be higher than the base material and friction stir welded specimens. High microhardness was attributed to the presence of both β -(Al, Fe, Si) and Al₂Cu phases.
- The cold metal transfer welded specimen was dominated by severe wear and the friction stir welded specimen was dominated by mild wear.
- Electrochemical corrosion test revealed that the corrosion rate of the cold metal transfer welded specimens was higher than that of the friction stir welded specimens, which was accredited to the presence of large volumes of inter-metallics with a significant difference in corrosion potential. The results are consistent with the immersion test results.

The results indicated that cold metal transfer welded specimens had high hardness, tensile strength, impact strength, and wear resistance than the friction stir welded specimens. However, the corrosion resistance of cold metal transfer welded specimens was lower than the friction stir welded specimens.

References

- [1] V. Sharma, K. S. Kumar, B. N. Rao, and S. Pathak, "Effect of microstructure and strength on the fracture behavior of AA2219 alloy," *Materials Science and Engineering A*, vol. 502, pp. 45-53, 2009.
- [2] S. Tosto, F. Nenci, and J. Hu, "Microstructure and properties of electron beam welded and post-welded 2219 aluminium alloy," *Materials Science and Technology*, vol. 12, pp. 323-328, 1996.
- [3] W. Xu, J. Liu, and H. Zhu, "Pitting corrosion of friction stir welded aluminum alloy thick plate in alkaline chloride solution," *Electrochimica Acta*, vol. 55, pp. 2918-2923, 2010.
- [4] G. Dance, "Comparative evaluation of mechanical properties of TIG, MIG, EBW and VPPA welded AA2219 aluminum alloy," *Welding and Metal Fabrication*, vol. 24, pp. 216-222, 1994.
- [5] S. Malarvizhi and V. Balasubramanian, "Fatigue crack growth resistance of gas tungsten arc, electron beam and friction stir welded joints of AA2219 aluminium alloy," *Materials and Design*, vol. 32, pp. 1205-1214, 2011.
- [6] S. Malarvizhi, K. Raghukandan, and N. Viswanathan, "Effect of post weld aging treatment on tensile properties of electron beam welded AA2219 aluminum alloy," *International Journal of Advanced Manufacturing Technology*, vol. 37, pp. 294-301, 2008.
- [7] D. Dittrich, J. Standfuss, J. Liebscher, B. Brenner, and E. Beyer, "Laser beam welding of hard to weld Al alloys for a regional aircraft fuselage design—first results," *Physics Procedia*, vol. 12, pp. 113-122, 2011.
- [8] P. B. Srinivasan, K. Arora, W. Dietzel, S. Pandey, and M. Schaper, "Characterisation of microstructure, mechanical properties and corrosion behaviour of an AA2219 friction stir weldment," *Journal of Alloys Compounds*, vol. 492, pp. 631-637, 2010.
- [9] C. G. Pickin, S. W. Williams, and M. Lunt, "Characterisation of the cold metal transfer (CMT) process and its application for low dilution cladding," *Journal of Materials Processing Technology*, vol. 211, pp. 496-502, 2011.
- [10] P. Almeida and S. Williams, "Innovative process model of Ti-6Al-4V additive layer manufacturing using cold metal transfer (CMT)," in *Proceedings of the twenty-first annual international solid freeform fabrication symposium, University of Texas at Austin, Austin, TX, USA*, 2010.
- [11] P. Wang, S. Hu, J. Shen, and Y. Liang, "Characterization the contribution and limitation of the characteristic processing

- parameters in cold metal transfer deposition of an Al alloy," *Journal of Materials Processing Technology*, vol. 245, pp. 122-133, 2017.
- [12] H. Zhang, S. Hu, Z. Wang, and Y. Liang, "The effect of welding speed on microstructures of cold metal transfer deposited AZ31 magnesium alloy clad," *Materials and Design*, vol. 86, pp. 894-901, 2015.
- [13] R. V. Vignesh and R. Padmanaban, "Modelling tensile strength of friction stir welded aluminium alloy 1100 using fuzzy logic," in *Intelligent Systems and Control (ISCO), 2017 11th International Conference on*, 2017, pp. 449-456.
- [14] R. V. Vignesh, R. Padmanaban, M. Arivarasu, S. Thirumalini, J. Gokulachandran, and M. S. S. S. Ram, "Numerical modelling of thermal phenomenon in friction stir welding of aluminum plates," *IOP Conference Series: Materials Science and Engineering*, vol. 149, p. 012208, 2016.
- [15] H. Fujii, L. Cui, M. Maeda, and K. Nogi, "Effect of tool shape on mechanical properties and microstructure of friction stir welded aluminum alloys," *Materials Science and Engineering A*, vol. 419, pp. 25-31, 2006.
- [16] M. Dehghani, A. Amadeh, and S. A. Mousavi, "Investigations on the effects of friction stir welding parameters on intermetallic and defect formation in joining aluminum alloy to mild steel," *Materials and Design*, vol. 49, pp. 433-441, 2013.
- [17] P. Cavaliere, A. De Santis, F. Panella, and A. Squillace, "Effect of welding parameters on mechanical and microstructural properties of dissimilar AA6082-AA2024 joints produced by friction stir welding," *Materials and Design*, vol. 30, pp. 609-616, 2009.
- [18] T. Chen and W.-B. Lin, "Optimal FSW process parameters for interface and welded zone toughness of dissimilar aluminium-steel joint," *Science and Technology of Welding and Joining*, vol. 15, pp. 279-285, 2010.
- [19] S. K. Rao, G. M. Reddy, K. S. Rao, M. Kamaraj, and K. P. Rao, "Reasons for superior mechanical and corrosion properties of 2219 aluminum alloy electron beam welds," *Materials characterization*, vol. 55, pp. 345-354, 2005.
- [20] V. V. Ramalingam and P. Ramasamy, "Modelling Corrosion Behavior of Friction Stir Processed Aluminium Alloy 5083 Using Polynomial: Radial Basis Function," *Transactions of the Indian Institute of Metals*, vol. 70, pp. 2575-2589, December 01 2017.
- [21] R. Vaira Vignesh, R. Padmanaban, and M. Datta, "Influence of FSP on the microstructure, microhardness, intergranular corrosion susceptibility and wear resistance of AA5083 alloy," *Tribology - Materials, Surfaces & Interfaces*, pp. 1-13, 2018.
- [22] Sivaraos, K. R. Milkey, A. R. Samsudin, A. K. Dubey, and P. Kidd, "Comparison between taguchi method and response surface methodology (RSM) in modelling CO2 laser machining," *Jordan Journal of Mechanical and Industrial Engineering*, vol. 8, pp. 35-42, 2014.
- [23] V. V. Ramalingam and P. Ramasamy, "Modelling Corrosion Behavior of Friction Stir Processed Aluminium Alloy 5083 Using Polynomial: Radial Basis Function," *Transactions of the Indian Institute of Metals*, vol. DOI: 10.1007/s12666-017-1110-1, April 11 2017.
- [24] V. Ramakoteswara Rao, N. Ramanaiah, and M. M. M. Sarcara, "Optimization of volumetric wear rate of Aa7075-Tic metal matrix composite by using taguchi technique," *Jordan Journal of Mechanical and Industrial Engineering*, vol. 10, pp. 189-198, 2016.
- [25] A. K. Jafarzadeh, T. Shahrabi, S. M. M. Hadavi, and M. G. Hosseini, "Role of Chloride Ion and Dissolved Oxygen in Electrochemical Corrosion of AA5083-H321 Aluminum-Magnesium Alloy in NaCl Solutions under Flow Conditions," *Journal of Materials Science & Technology*, vol. 23, 2007.